



ZnO/TiO₂ nanocomposites semiconductor for anti-bacterial applications and dye sensitized solar cell applications

N. Geetha¹, S. Sivarajani^{1,2}, A. Ayeshamariam^{1,3,*}, Mariadhas Valan Arasu⁴, N. Punithavelan⁵

¹Research Scholar, Bharathiyar University, Coimbatore, 641046, India

²Department of Physics, SBM College of Engineering Technology, Dindigul, India

³Department of Physics, Khadir Mohideen College, Adirampattinam, Tamilnadu, 614701, India

⁴Department of Botany and Microbiology, Addiriyah Chair for Environmental Studies, College of Science, King Saud University, Riyadh, Kingdom of Saudi Arabia

⁵School of Advanced Sciences in Physics, Vellore Institute of Technology Chennai Campus, Chennai, Tamilnadu, India

*) Email: aismma786@gmail.com

Received 22 April 2018, Accepted 30 Aug. 2018, Accepted 15 Sep. 2018

The synthesis of high quality ZnO doped TiO₂ nanoplatelets were synthesized by hydrothermal method at room temperature (RT). Composition, structure and micro morphology of the nanoplatelets were analyzed and determined by X-ray diffraction (XRD) confirms that crystal structure of doped (Zn-Ti-O) composition the identify peaks of (002), (100) and (101) clearly showed hexagonal wurtzite-type structure of ZnO with same lattice constants of the same; a=b=3.249 Å and c= 5.219 Å. From the XRD results revealed that crystal properties of the doped samples are improved without affecting the parent lattice. The morphological and optical properties of Zn-Ti-O nanosamples were characterized by scanning electron microscopy (SEM). TEM observation shows that the ZnO/TiO₂ nanoplatelets synthesized by hydrothermal synthesis are well dispersed and the average crystallite size was found to be 10 nm. Biological applications of bacterial strains were calculated for these samples. The antibacterial activity of ZnO/TiO₂ and its doping was evaluated on bacteria strains like *Escherichia coli*, *Pseudomonas aeruginosa* and *Staphylococcus aureus*. The results obtained in this study suggested that the ZnO/TiO₂ and its doping have potential for use in the treatment of diseases caused by these test organisms.

Keywords: Nanoplatelets; Colloidal processing; TiO₂; ZnO and biological strains

1. INTRODUCTION

ZnO/TiO₂ nanostructure is one of the most important transparent semiconducting metal oxides (TCMOs) compounds in the field of material science due to the wide range applications of solar cells, solar cell batteries, biological sensors, gas sensor and flat-panel displays (FPDs) which are unique optical and electrical properties have been extensively studied in the fields of photo-electronic, electrochemical materials etc. Zinc Oxide (ZnO) compound belongs to IV group attracted great attention for the preparation of devices related to the optical because of the presence of band gap (3.34 eV), enlarged excitation binding energy (60 meV), and higher optical activity. Moreover, Titanium dioxide (TiO₂) is a very useful functional material due to its semiconductive properties, physical and chemical stability, cost effective fabrication material biocompatibility and high corrosion resistance made TiO₂ one of the most used materials in various industrial applications. Nowadays, ZnO is also used as a photo anode in the dye-sensitized solar cell (DSSC) and highest achieved efficiency is about 0.28 % efficiency. In chemically doped TiO₂ with ZnO crystallites *are* capable of generating photocurrents under visible light radiations which is high transparence with elevated light trapping characteristics guarantees with efficient ultraviolet emission. Actually, the higher conductivity of ZnO-based nanoplatelets, various tetravalent metal dopants is added to ZnO nanoparticles, such as Ti, Sn, Ga and Si etc. Among the other possible oxides, Nb₂O₅, CdO, PbO and SiO₂ are for many applications. Titanium (Ti) is the most promising doping element among these tetravalent metal dopants since ionic radii of Ti²⁺ are equal to Zn²⁺ and hence it can easily be substituted into Zn sites within Ti host lattice. The dopant Ti provides two more free electrons (Zn²⁺ is replaced by Ti²⁺), the electrical conductivity would be improved. Even if expensive not available in abundance, a number of semiconductors are well suited in powder form for its bacterial and fungal applications on a large scale. Many reports have used for the evaluation of the harmful effects of titanium dioxide nanoparticles in biological studies, but few reports have based on the DSSC (Dye Sensitized Solar Cell) applications of it. Thermodynamic modelling shows an increase in gas generation with an increase of the fuel-oxidant. The performance of these materials being studied presently is to identify their bacterial activities of positive and negative microbial strains *Escherichia coli*, *Pseudomonas aeruginosa* and *Staphylococcus aureus* which is reported here.

2. EXPERIMENTAL PROCEDURE

Titanium oxide (TiO₂) doped zinc oxide (ZnO) nanopowder was synthesized by hydrothermal method. 0.5 M solution of Zinc acetate dehydrate is dissolved in distilled water of 25 ml, TiO₂ solution in different beakers with same volume, this mixture was mixed with 0.26 gm of glycine which acts as a fuel. This mixed solution was stirred for 20 minutes by using magnetic stirrer. After that the material was autoclaved for 15 h. Further, the material was cleaned using sterile dried using vacuum for 36 h. The prepared samples were powdered and further washed using distilled water and ethanol for three times and dried in vacuum at 70 °C for 5 hrs. Zinc acetate dehydrate was doped with the ratio of Titanium Oxide salts in the ratio of (90:10), 10% of TiO₂ is doped with Zinc acetate dehydrate. Titanium oxide powdered salt was doped with Zinc acetate dehydrate of 10%. These mixtures were synthesised again by Hydrothermal

synthesis, this mixture was dissolved with Glycene of same 0.26 gm. The X-ray powder diffraction (XRD) was performed by following the standard methodology using DSSC based on nanocrystalline mesoporous ZnO-TiO₂ NPs have attracted much attention as potential low-cost alternative for single or polycrystalline p-n junction silicon solar cells. DSSCs (Dye Sensitised Solar Cells) can reach solar to electrical energy conversion efficiencies above 10%. Upon illumination, photons are absorbed by dye molecules, which inject electrons from their excited states in to the conduction band of the Zinc-titania nanoparticles. The low-absorption coefficient of a dye monolayer is compensated by the mesoporous structure of the ZnO-TiO₂ NPs, which leads to a strong increase in the number of ZnO/TiO₂/dye/electrolyte interfaces through which photons pass, thus increasing the absorption probability.

3. RESULTS AND DISCUSSION

The XRD diffraction pattern of TiO₂ doped ZnO nanoplatelets which gives information about the average crystallite size and it was estimated via Debye-Scherer's formula

$$D = 0.9\lambda/\beta\cos\theta \quad (1)$$

where D presents average crystallite size; λ depicts the wavelength of X-ray used (0.154 nm), β implies the full width at half maximum (FWHM); and θ infers Bragg's angle. Herein, the doping is accompanied to replace dopant atoms i.e., Zn²⁺ ions are effectively consolidated within ZnO lattice by occupying Ti⁴⁺ without varying the parent crystal structure. Instead of that, the proportionate strain is reduced further in the lattice site. The dislocation density of the pure crystal is greater than doped one which is observed in both cases. The crystal sizes of TiO₂ doped ZnO nanoplatelets are 36.25, 36.90, 33.67 and 34.02 respectively as shown in Fig. 1(a-d). It seems that the crystal size (grain size) is decreased by the effect of doping, in both cases. The decrease of crystallite size with doping is owing to the improved density of nucleation centers at the time of layer growth and also improved lattice disorder as a outcome of the ionic radius alteration between Ti⁴⁺ and Zn²⁺ [14-15].

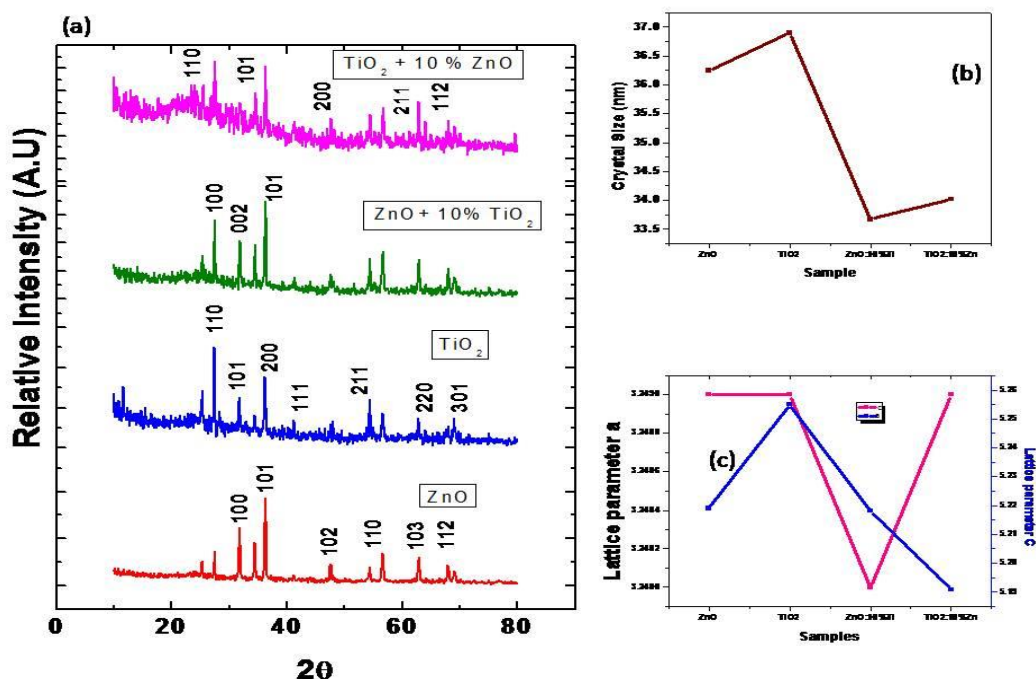


Figure 1 (a-c). XRD diffraction pattern of TiO₂ doped ZnO nanoplatelets

Figure. 1b, showed that ZnO existed in both the form of cubic zinc blende and hexagonal wurtzite structure. XRD pattern of the present compound showed the peaks corresponding to cubic as well as hexagonal geometrical planes (002), (100), (101), (102), (103), (110) and (112) which might be due to doping of TiO₂ with ZnO material. It is observed that covalent bonds are formed electrochemically between TiO₂ and ZnO compounds and Ti and Zn are directly coupled with O-atoms in the crystal lattice. The corresponding peak positions of TiO₂ doped ZnO nanoplatelets observed peaks from the interplanar spacing are (002), (100) and (101) clearly showed hexagonal wurtzite-type structure of ZnO with same lattice constants of the same; a=b= 3.249 Å and c= 5.219 Å also ensure the lattice formation which consistent with the standard diffraction spectrum of JCPDS card (37-1451). The corresponding diffraction peaks of the wurtzite ZnO were only detected, suggesting that the TiO₂ has arrived ZnO lattice without altering its original structure. Fig. 1(c) displays the ZnO structure with lattice parameters in comparison with the TiO₂ doped ZnO and estimated that the unit cell parameters a (3.249 Å) and c (5.219 Å). The remarkable interpretations from the results argued above are multifold. The upsurge in the lattice parameter and crystallite size, the formation of ZnO pattern in doping percentage and the noticeable shift in the some of the peak position are the prominent differences. These results conclude the formation of single phase of TiO₂ rather than individual phases.

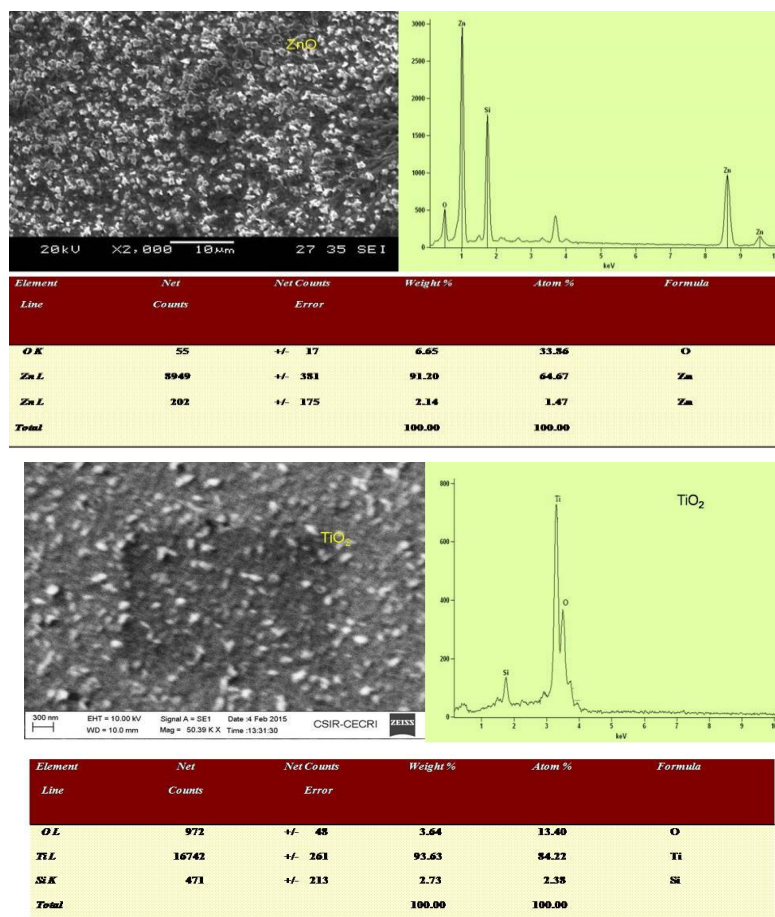


Figure 2(a,b) show EDAX spectra of ZnO, **Figure 3(a,b)** TiO₂ and its nanocomposites

Figure 4(a,b) ZnO doped with TiO₂ (90:10) and **Figure 5(a,b)** TiO₂ doped with ZnO (90:10) where only Ti, O and Zn elements are tabulated in Table 1. Addition Ti content into ZnO matrix and Zn content into TiO₂ matrix was confirmed from the observed EDAX spectra. Figure 2(a-b) SEM and EDAX analysis of ZnO nanoparticles Even though we were intended to add 10 at % of ZnO into TiO₂, and 10% of TiO₂ into ZnO. In ZnO the atomic weight percentages of Zn is 64.67% and O is 33.86% in TiO₂ Ti is 84.22 and O is 13.40, in the nanocomposites of ZnO: 10% TiO₂ Zn 77.56 at. % , Ti 2.20 (doping concentration of 10%) and O as 21.24% were entered into the system, remaining was washed away during synthesis. TiO₂: 10% ZnO nanocomposite, the stoichiometric atomic percentage of Ti as 58.76, Zn 17.04 Zn, O were observed 24.20 respectively.

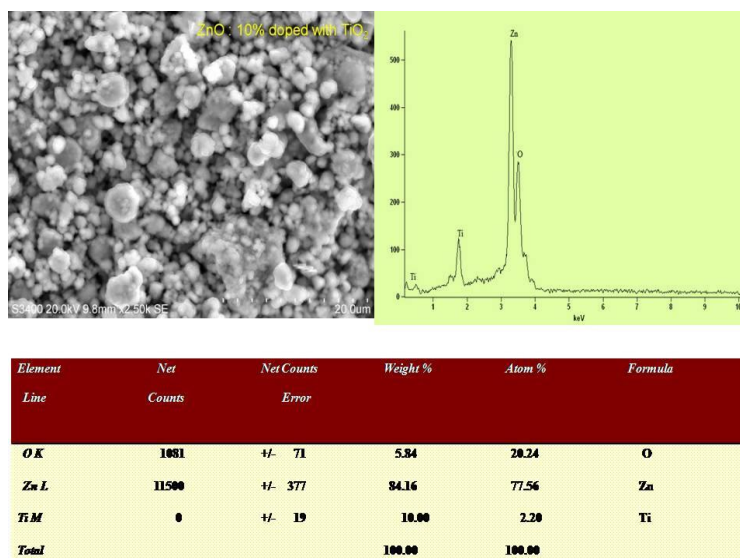


Figure 4(a-b) SEM and EDAX analysis of TiO₂ nanoparticles

All the samples ZnO, TiO₂ and doping nanocomposites showed much oxygen deficiency. The morphology of the nanoparticles and its nanocomposites were cubic in size except the TiO₂: 10% ZnO of nanocomposites. It showed the rod shaped morphological structures.

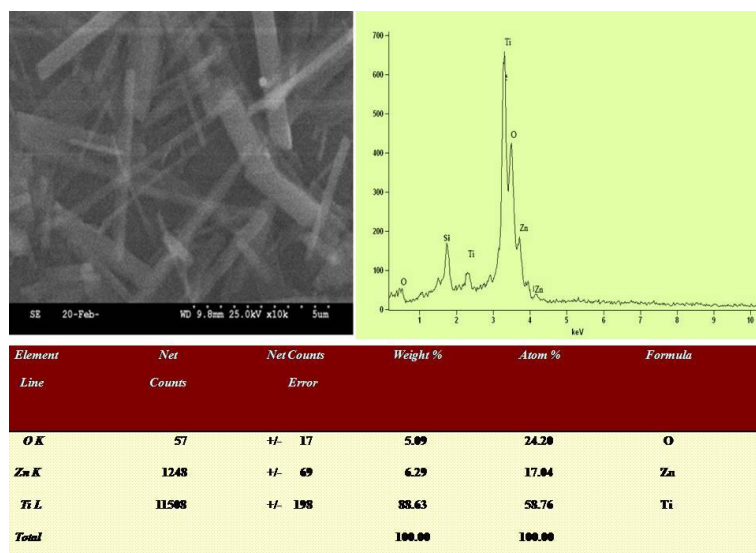


Figure 5(a-b) SEM and EDAX analysis of ZnO: 10% TiO₂ nanocomposites

Compositions were synthesized using Hydrothermal synthesis technique and the influence of annealing temperature on their structures was analyzed. The XRD results revealed that particle size increases for the nanocomposites of TiO₂: 10% ZnO and decreases with increase of ZnO content ie ZnO: 10% TiO₂. Nanoparticles than nanocomposites without any secondary phases for ZnO and TiO₂ samples. As a subsidiary result, crystal size calculated from XRD and TEM technique

(Which includes phonon confinement) shows better accuracy for particle size than XRD measurements of nanoparticles and nanocomposites [16-18]. Figure 5(a-b) SEM and EDAX analysis of TiO₂ : 10% ZnO nanocomposites the high-resolution transmission electron microscopy (HRTEM) of TiO₂ doped ZnO nanoplatelets were prepared by hydrothermal method. It is obvious from Figure. 6(a-h) showed that the XRD and SAED patterns are densely deposited, and the average size of the grains is about ~ 5 nm. In order the high magnification HRTEM images in Figures. 2(a,b), 3(a,b), 4(a,b) and shows that the spherical aggregates have decent crystallinity and are composed of nanoparticles with a diameter less than 25 nm, which is in good agreement with earlier XRD studies. A high-resolution SAED analysis reveals that lattice fringes on the crystal face have a spacing of 3.249 Å, agreeing to the (101) face of ZnO. This indicates that the hexagonal ZnO nanoplatelets arrays in a large scale, growing almost perpendicular to the surface morphology, which is composed of densely packed highly oriented nanoplatelets with diameter in the range (5–10) nm.

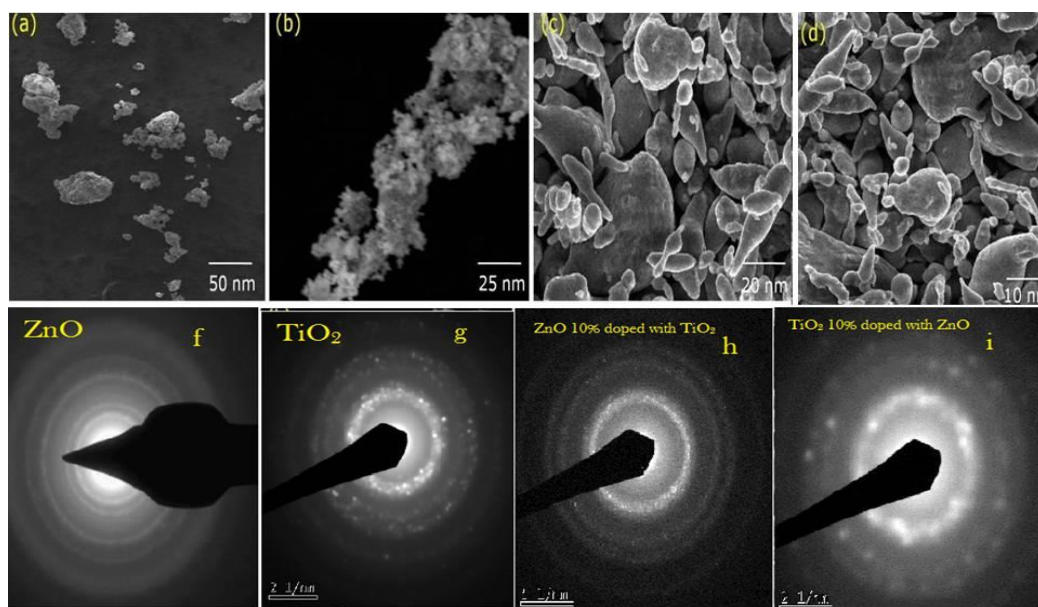


Figure 6(a-h) TEM and SAED pattern of ZnO, TiO₂, ZnO:10% TiO₂ and TiO₂: 10% ZnO nanocomposites

Moreover, this nanocrystals exhibits a highly c-axis preferred orientation, consistent with the XRD results. Also, the highly oriented nanoplatelets in the TiO₂ doped ZnO nanoplatelets are denser. Conversely, increasing the amount of ZnO leads to reduce the density whereas upsurge the diameter of nanoplatelets as displayed in Fig. 6 (a, b), and c which exposes the information about the diameter and length of nanoplatelets [19-22]. Furthermore, the morphology is transformed into the uniform multi-oriented platelets with incorporation of TiO₂. TiO₂ doped ZnO nanoplatelets show a multi-oriented spear-like structure Fig. 4(c-e). The diameter of these platelets varies from approximately 50 nm to 5 nm.

Table 1 Structural and bandgap values of TiO₂ doped ZnO nanoplatelets.

Sample	Lattice parameter		Crystal Size (nm)	Strain 10 ⁻⁴	Dislocation density x 10 ¹⁴ lines/m ²	Bandgap (eV)
ZnO	3.249	5.219	36.25	3.506	7.612	3.206
TiO ₂	3.239	5.255	36.90	3.573	7.602	3.073
ZnO- (10 %) TiO ₂	3.248	5.218	33.67	3.895	7.489	2.995

TiO ₂ - (10 % ZnO)	3.247	5.191	34.02	3.905	7.512	2.605
-------------------------------	-------	-------	-------	-------	-------	-------

The results indicate that ZnO nanoplatelets can be effectively fabricated by the hydrothermal method, and the size, density and orientation of these nanoplatelets can be controlled by incorporating ZnO dopant. SAED pattern 6(a-h) of ZnO, TiO₂, ZnO 10% doped with TiO₂ and TiO₂ doped with ZnO nanoparticles well matched with the diffraction pattern of XRD peaks figure 1(a-b) [23-26].

Bacterial Studies

The antimicrobial properties of TiO₂, ZnO, Ti doped ZnO and ZnO doped TiO₂ composites are depicted in Figure 7(a-d).

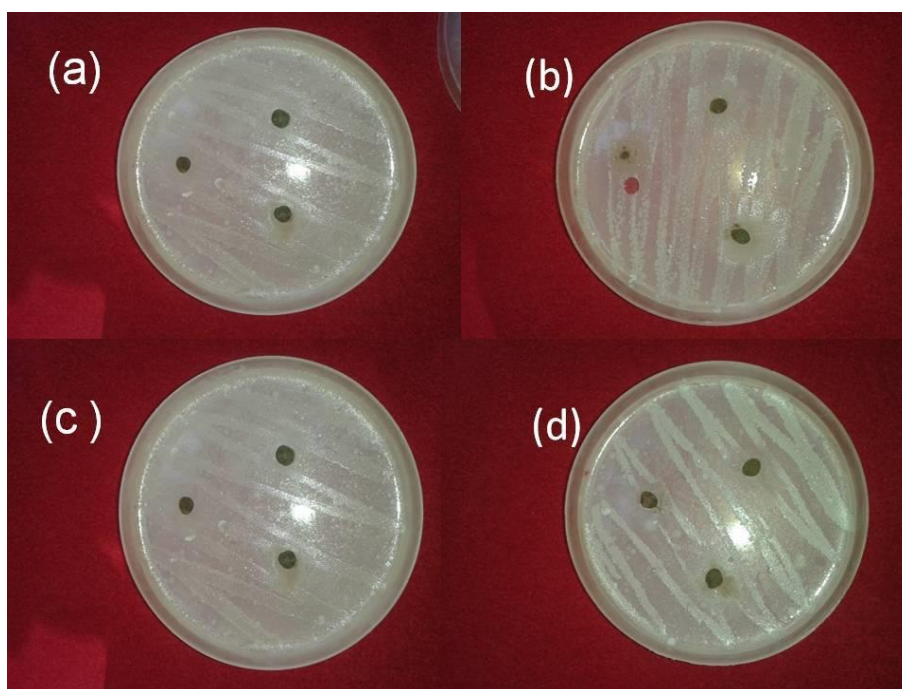


Figure 7(a-d) Biological studies of ZnO, TiO₂, ZnO:10% TiO₂ and TiO₂: 10% ZnO nanocomposites.

The zone of inhibition of both Gram positive and Gram negative microbial strains against these studied materials clearly confirmed that the activity was directly proportional to the concentration of ZnO and TiO₂ composite. The result shows that there is no inhibition on bacterial growth when the glass plate contains TiO₂, ZnO, Ti doped ZnO and ZnO doped TiO₂ composites. Under room light condition, the powder of TiO₂, ZnO, Ti doped ZnO and ZnO doped TiO₂ composites are used to examine its effects on the antibacterial activity for negative and positive bacteria. Gradually the zone of inhibition of both pathogens increased with the increase of the doping concentration of TiO₂. Due to increasing the TiO₂ content in the composites the results shown in the histogram of Figure 7(a-d). Among the microbial strains Gram positive strains were more susceptible to the studied compounds than Gram negative

strains. It is evidenced that Gram negative microbial strains contained thick cell wall membrane and lipopolysaccharides such substance stop the penetration of the material into the cells [27-28]. Despite the ZnO compound exhibited higher inhibitory activities of positive and negative biological strains, the antibacterial activity was high for ZnO than TiO₂ shown in Figure 8(a-b). The MIC result is traceable to the fact that the two fold serial dilution reduced its initial concentration of 0.1mg/ml which had no visible effect in ZnO-TiO₂ sample than TiO₂-ZnO on the organisms resulting in different zone of inhibition which is shown in Figure 7(c-d). Water and ethanol were used as the solvent. The antibacterial activity of these four samples was performed by agar disc diffusion method. The antibacterial effect of aqueous extract showed a zone of inhibition on *Escherichia coli*, which was (1-5) millimeter in diameter. The ethanol extract also showed little zones of inhibition on the test organisms ranging from (1-5) mm in diameter. Efficient utilization of solar energy is the main goal of modern technology. Several concepts are available for solar to electricity conversion, low cost dye sensitized solar cell is one of the alternate to conventional solar cells. Dye-sensitized solar cell s (DSSC) by using TiO₂ and doping of ZnO nanocomposites will be expected to be the next-generation solar cell because they can be fabricated at a low cost and use no harmful materials. It is necessary to improve electrolyte for improvement of long-term stability and reliability of the cells of ZnO and TiO₂ nanocomposites. For the fabrication of dye sensitized solar cells (DSSC), dye solution can be obtained by dissolving various photosensitive dyes which act as photosensitizer, in a solvent. The photosensitizing dye (Methylene blue) has absorptions in various visible and IR regions.

For efficient functioning of the system, the used dye should be strongly adsorbed on the semiconductor layer. Methylene blue is used as the dye here for ZnO and TiO₂ doping of nanocomposites DSSC solar cells [29]. The aqueous solutions, alcohols such as ethanol was used as solvents. These solvents can be used either individually or under mixture with methanol, such as acetone, ether such as diethyl ether. Concentration of dye depends on the type of dye and solvent used. Dye can be adsorbed on the semiconductor layer by dipping it in the dye solution under ambient conditions for about 5 minutes to 96 hours. A DSSC is an electrochemical solar cell that includes an electrode with an oxide layer having dye molecules chemically absorbed onto the surface there of. The dye molecules absorb visible rays to produce electron-hole pairs and the electrode transfers the produced electrons. DSSC efficiency mainly based on work function of semiconductors, dye and electrolyte solution. ZnO: 10% TiO₂ and TiO₂ : 10% ZnO was constrained by the energy levels of the dye with respect to conduction band edge and the efficiency of the electron transfer from the dye.

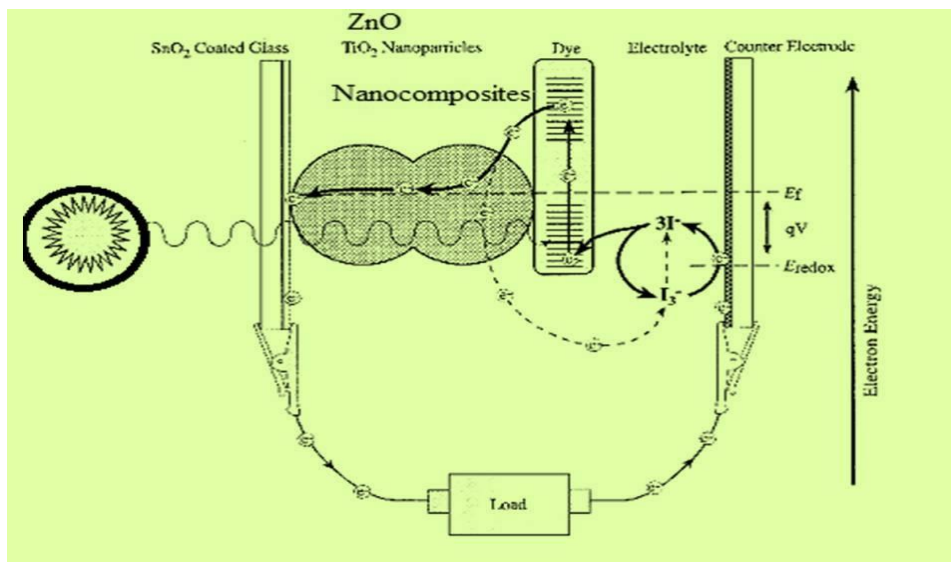


Figure 8. Working mechanism of dye sensitized solar cell

The semiconductor. Dye sensitised solar cell based on different morphology of the pure semiconductor oxides provides improvement in the electron transport by providing direct conduction pathways to substrate. In the mixed semiconductor systems, binary $\text{TiO}_2:\text{ZnO}$ nanocomposites have received considerable interest, due to high reactivity of TiO_2 and large exciton binding energy of ZnO . TiO_2 has some defects such as fast recombination of photogenerated electron/hole pair and high photocatalytic activity under UV light of sun, which decomposes the organic compounds in the cell during usage, so it has shortterm reliability. These limitations become bearable when dye sensitized nanocomposites are used as solar cell material [30,31]. Pinch of dye was dissolved in 20 ml of ethanol to obtain dye solution. Synthesized nanocomposite powders were added with the as prepared dye solution and aged for 24 hours to obtain dye adsorbed nanocomposites. Ethanol was chosen as solvent so as to have better adherence of dye with the surface of nanocomposites.

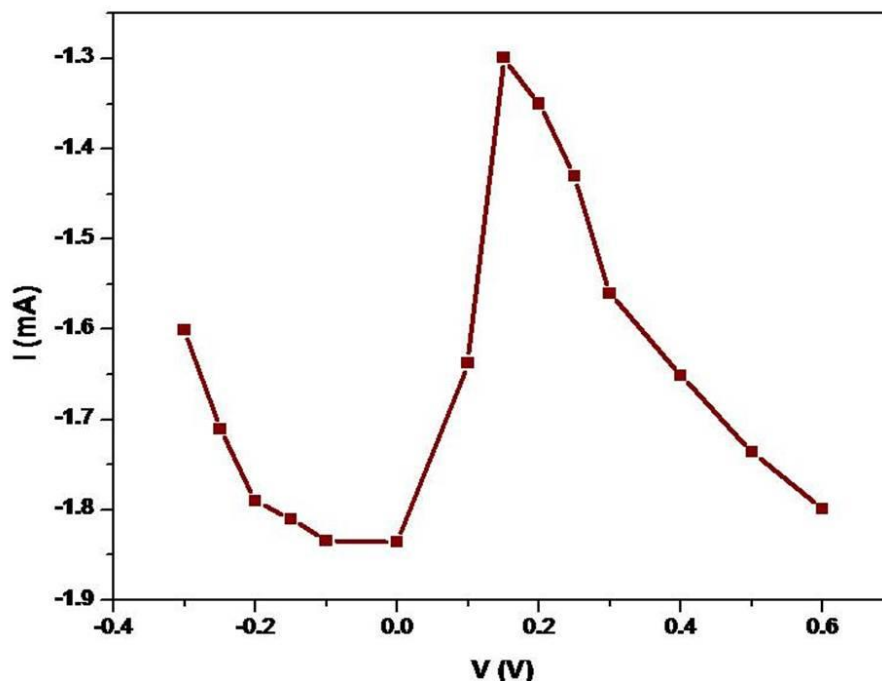


Figure 9. I-V performance of nanocomposite annealed at 250 °C.

ZnO, TiO₂ nanoparticles ZnO: 10% TiO₂ and TiO₂: 10% ZnO nanocomposite powder prepared using Hydrothermal analysis was used here, 0.127 g of iodine were added into 10 ml of ethylene glycol and stirred for 15 minutes. 0.83 g of potassium iodine was added to the same solution with further stirring for 5 minutes. The prepared electrolyte was stored in dark container with a tight lid. Fluorine doped tin oxide conductive glass slides were taken and its conductive side were tested using multimeter. 0.5 g of ZnO, TiO₂ nanoparticles ZnO: 10% TiO₂ and TiO₂: 10% ZnO nanocomposite powder were taken in a mortar and pestle and grounded it for 30 minutes with addition of few drops of acetic acid sequentially to obtain colloidal form. To which one drop of surfactant was added (soap oil) to facilitates their spreading on the FTO substrate [32]. After testing, one of the glass slides was masked on three sides with masking tape to form a mold. A couple of drops of nanocomposites suspension was then added and distributed across the area of the mold with glass rod. The slide was then set aside to dry for 10 minutes. After the first slide has dried, tape was removed and the coated layer was allowed to calcination at 250°C for 10 minutes in atmosphere. Pinch of Methylene blue dye was dissolved in 5 ml of ethanol to get dye solution. By allowing the calcinated slide to cool at room temperature, place the slide face down in the dye solution and allow it to be absorbed for 5 minutes. Conductive side of the second slide was placed over an open flame and move back and forth. This will coat the second slide with a carbon catalyst layer. Two slides were placed together, so that two layers are touching. Binder clips were used to keep two slides together. One drop of electrolyte solution was added between the slides so as to have capillary action. Dye sensitised Solar cell comprises of wide band gap semiconductor oxide film (photo anode), dye sensitizer, electrolyte and counter electrode. The film adsorbs light harvesting dye molecules. When these dye molecules absorb light, they are excited from ground state to excited state. Excited dye molecules inject electrons to the conduction band of the semiconductor. The injected electrons diffuse through the semiconductor thin film to the transparent conducting FTO substrate. Subsequently, the electrons flow through the load via the external circuit and then reach the counter electrode. The resultant oxidized dye molecules are quickly reduced back by I⁻ ions in

the electrolyte. This process is called the dye regeneration. The electrolyte in turns obtains an electron from the catalyst coated counter electrode. This is repeated to obtain electric energy from the Dye sensitised solar cell. The working mechanism of dye sensitized nanocomposite is shown in Figure 10 [33].

Photo Current–Voltage curve was recorded using Newport solar simulator model under two electrode systems. Xenon lamp was used as a light source. Incident light intensity was maintained at 100 mW/cm². The I-V performance of the dye sensitized ZnO, TiO₂, ZnO: 10% TiO₂ and TiO₂: 10% ZnO nanocomposite annealed at 250°C was shown in Figure 10. To avoid the excitation of UV light on ZnO, TiO₂, ZnO: 10% TiO₂ and TiO₂: 10% ZnO nanocomposite semiconductor, filters were used to cut off light of particular wavelength range. The effective area of the cell was 0.8 cm X 0.5 cm. Under the irradiation of nanocomposites, the overall conversion efficiency of the cell was calculated and shown in Table 2.

The power conversion efficiency is given as

$$\eta = \frac{I_m V_m}{P} \times 100\% \quad (2)$$

where, $I_m V_m$ is the maximum multiplied value in I-V sweep and P is illumination power input (100 mW/cm²). Using Equation. (2) the power conversion efficiency of the Dye-Snsitised Solar Cell was calculated as 1.63 %. The dye sensitized ZnO: 10% TiO₂ and TiO₂: 10% ZnO photoelectrodes with electrolyte shows consistent photocurrent than without electrolyte, suggesting that electrolyte is important for effective charge transport and to protect the device from drying. Figure 11 shows I-V curve of nanocomposite with the addition of electrolyte. From that we observed the photocurrent as 1.71 and 1.65 mA [34].

Table 2 Parameters determined from I-V characteristics curve.

Material	I _m (mA)	V _m (V)	η %
ZnO: 10% TiO ₂	1.65	0.39	1.59
TiO ₂ : 10% ZnO	1.71	0.42	1.63

This indicates the significance of electrolyte. Grain size, amount of dye adsorbed and the type of electrolyte affects the overall performance of the cell. ZnO played an important role in electron transport, so the loss of photocurrent due to lower of dye adsorbed on composite film can be compensated sufficiently [35]. The energy level for electron injection is decreased after ZnO covered on the surface of TiO₂ particle, which increases the driving force for electron injection and hence reduce recombination between injected electron and accepted electrons such as dye cation or iodine ions. The Table 2 results show that charge recombination can be reduced upon the surface modification of TiO₂ with ZnO. This implies that number of deep trap states existing in the surface of TiO₂ is decreased and after addition of ZnO electron gets transported much faster [36].

4. CONCLUSIONS

ZnO, TiO₂ and ZnO: 10% TiO₂ and TiO₂: 10% ZnO nanoplatelets were synthesized by hydrothermal method. Molecular structure of all nanoplatelets samples was analyzed the lattice variations are different cannot be detected its molecular region of Ti with ZnO. Dye sensitized nanocomposites were synthesised using Methelyene blue dye. Now nanocomposite ZnO: 10%

TiO₂ and TiO₂ : 10% ZnO were used for solar cell fabrication. The I-V performance of the dye sensitized ZnO: 10% TiO₂ and TiO₂ : 10% ZnO electrode shows 1.63 % and 1.59% device power conversion efficiency. Recent developments in the area of sensitizers for these devices have led to dyes which absorb across the visible spectrum leading to higher efficiencies. The recent development of an all dye sensitised solar cell holds additional potential for further cost reduction and simplification of the manufacturing of dye solar cells.

Acknowledgment

The Project was full financially supported by King Saud University, through Vice Deanship of Research Chairs

References

- [1] J. Kolnik, M. Ozvold, Phys. Stat. Solidi (a) 122 (1990) 583
- [2] E. H. Rhoderick, *Metal semiconductor contacts*, Oxford University Press Oxford (1978)
- [3] K. Kaviyarasu, E. Manikandan, J. Kennedy, M. Maaza, RSC Adv. 5 (2015) 82421
- [4] A. Ayeshamariam, M. Kashif, S. Arokiyaraj, M. Bououdina, M. G. Sankaracharyulu, M. Jayachandran, U. Hasim 9-3 (2014) 1007
- [5] T.V. Vimalkumar, N. Poornima, C. Sudha Kartha, K.P. Vijayakumar, Mater. Sci. Eng. B. 175 (2010) 29
- [6] M. Fouzri, A. Boukadhaba, M. Oumwzzine, Thin Sol. Films 520 (2012) 2582
- [7] N.L. Tarwal, V.V. Shinde, A.S. Kamble, P.R. Jadhav, D.S. Patil, V.B. Patil, P.S. Patil, Appl. Surf. Sci. 257 (2011) 10789
- [8] K. Kaviyarasu, E. Manikandan, J. Kennedy, M. Jayachandran, Mat. Lett. 120 (2014) 243
- [9] S. Ilican, Y. Caglar, M. Caglar, J. Optoelectron. Adv. Mater. 10 (2008) 2578
- [10] S. Flickyngerova, K. Shtereva, V. Stenova, D. Hasko, I. Novotny, V. Tvarozek, P. Sutta, E. Vavrinsky, Appl. Surf. Sci. 254 (2008), 3643
- [11] H. Wang, R. Bhattacharjee, I.M. Hung, L. Li, Electrochim. Acta 111 (2013) 797
- [12] Law, M., Greene, L. E., Radenovic, A., Kuykendall, T., Liphardt, J., & Yang, P. The Journal of Physical Chemistry B 110 (2006) 22652
- [13] K.J. Chen, F.Y. Hung, Y.T. Chen, S.J. Chang, Mater. Trans. 51 (2010) 1340
- [14] K. Kaviyarasu, C. Maria Magdalane, A. Anand, E. Manikandan, M. Maaza Spectro. Acta. Part A: Mol. & Biomol. Spect. 142 (2015) 405
- [15] Wang, Meili, Changgang Huang, Yongge Cao, Qingjiang Yu, Wang Guo, Qiufeng Huang, Yuan Liu et al. Applied Physics Letters 26 (2009) 263506
- [16] Manthina, V., Correa Baena, J. P., Liu, G., & Agrios, A. G. Journal of Physical Chemistry C 116 (2012) 23864
- [17] S. Vadivel, G. Rajarajan. Journal of Materials Science: Materials in Electronics 5 (2015) 3155
- [18] C.S. Prajapati, Ajay Kushwaha, P.P. Sahay, Materials Chemistry and Physics 142 (2013) 276
- [19] Manthina, Venkata, Juan Pablo Correa Baena, Guangliang Liu, Alexander G. Agrios..Journal of Physical Chemistry C 116 (2012) 23864

- [20] J. Zuo, C. Xu, X. Liu, C. Wang, C. Wang, Y. Hu, Y. Qian, J. Appl. Phys. 75 (1994) 1835
- [21] A. Ayeshamariam, S. Ramalingam, M. Bououdina, M. Jayachandran, Spectro. Acta. Part A: Mol. & Biomol. Spect. 118 (2014) 1135
- [22]. A. Ayeshamariam, M. Kashif, S. Muthuraja, S. Sivaranjani, C. Sanjeeviraja, M. Bououdina, J. Kor. Phy. Soc. 64 (2014) 254
- [23] Mariadhas Valan Arasu, Naif Abdullah Al-Dhabi, Valsalam Saritha, Veeramuthu Duraipandiyan , Chinnasamy Muthukumar and Sun-Ju Kim, Microbiology 13 (2013) 105
- [24] K. Kaviyarasu, E. Manikandan, M. Maaza, J. Alloys & Com. 648 (2015) 559
- [25] M. Kashif, I. Khaliq. International Journal of Agriculture and Biology 6 (2004) 138
- [26] G. Kiruthigaa, C. Manoharan, M. Bououdina, S. Ramalingam, C. Raju, Sol. St. Sci. 44 (2715) 32
- [27] S.S. Shinde, A.P. Korade, C.H. Bhosale, J. Alloys Com. 551 (2013) 688
- [28] Mariadhas Valan Arasu, Veeramuthu Duraipandiyan, Savarimuthu Ignacimuthu. Chemosphere 90 (2013) 479
- [29] Hussain Shahid et al. Materials Letters 118 (2014) 165
- [30] B. Li, L. Wang, B. Kang, P. Wang, Y. Qiu, Solar Energy Materials and Solar Cells 90 (2006) 549
- [31] D. I. Suh, S. Y. Lee, T. H. Kim, J. M. Chun, E. K. Suh, O. B. Yang, S. K. Lee, Chemical Physics Letters 442 (2007) 348
- [32] J. H. Yoon, S. R. Jang, R. Vittal, J. Lee, K. J. Kim, Journal of Photochemistry and Photobiology A: Chemistry 180 (2006) 184
- [33] P. J. Morrow, Nanotechnology Applications in Photovoltaic Technologies: Dye Sensitized Solar Cells. da Vinci's Notebook 9 (2012) 4
- [34] Du Pasquier, Aurelien, Hanhong Chen, Yicheng Lu, Applied Physics Letters 89 (2006) 253513
- [35] R. S. Mane, W. J. Lee, H. M. Pathan, S. H. Han, Journal of Physical Chemistry B 109 (2005) 24254
- [36] A. Qurashi, J. H. Kim, Y. B. Hahn. Superlattices and Microstructures 48 (2010) 162

© 2018 The Authors. Published by IFIA (<https://etn.iraqi-forum2014.com/>). This article is an open access article distributed under the terms and conditions of the Creative Commons Attribution license (<http://creativecommons.org/licenses/by/4.0/>).